



Non-viral vector mediated CKb11 with folic acid modification regulates macrophage polarization and DC maturation to elicit immune response against cancer

Wen Nie^{a,b,1}, Ting Yu^{c,1}, Xiaoxiao Liu^d, Bilan Wang^e, Tingting Li^a, Yin Wu^a, Xikun Zhou^a, Lu Ma^a, Yunfeng Lin^{f,g}, Zhiyong Qian^a, Xiang Gao^{a,*}

^a Department of Neurosurgery and Institute of Neurosurgery, State Key Laboratory of Biotherapy and Cancer Center, West China Hospital, West China Medical School, Sichuan University and Collaborative Innovation Center for Biotherapy, Chengdu, 610041, PR China

^b Department of Medical Oncology, The First Affiliated Hospital, School of Medicine, Zhejiang University, Hangzhou, 310003, China

^c Department of Pathology and Laboratory of Pathology, State Key Laboratory of Biotherapy, West China Hospital, West China School of Medicine, Sichuan University, China

^d Department of Radiation Oncology, Cancer Center, Affiliated Hospital of Xuzhou Medical University; Jiangsu Center for the Collaboration and Innovation of Cancer Biotherapy, Cancer Institute, Xuzhou Medical University, Xuzhou, 221000, China

^e Department of Pharmacy, West China Second University Hospital of Sichuan University, Chengdu, 610041, China

^f State Key Laboratory of Oral Diseases, National Clinical Research Centre for Oral Diseases, West China Hospital of Stomatology, Sichuan University, Chengdu, 610041, China

^g College of Biomedical Engineering, Sichuan University, Chengdu, 610041, China

ARTICLE INFO

Keywords:

Cancer
Immunogene therapy
CKb11
Nanocomposites
Macrophages polarization

ABSTRACT

The immunosuppressive tumor microenvironment (TME) of cancer strongly hinders the anti-tumor immune responses, thereby resulting in disappointing responses to immunotherapy. Chemoattractive and promotive traits of chemokines exerted on leukocytes have garnered interest in improving the efficiency of immunotherapy by increasing the infiltration of immune cells in the TME. In this study, a folic acid (FA)-modified gene delivery system based on the self-assembly of DOTAP, MPEG-PCL-MPEG, and FA-PEG-PCL-PEG-FA, namely F-PPPD, was developed to deliver plasmids encoding the immunostimulating chemokine CKb11. The delivery of plasmid CKb11 (pCKb11) by F-PPPD nanoparticles resulted in the high secretion of CKb11 from tumor cells, which successfully activated T cells, suppressed the M2 polarization of macrophages, promoted the maturation of dendritic cells (DCs), facilitated the infiltration of natural killer (NK) cells and inhibited the infiltration of immunosuppressive cells in tumor tissues. Administration of F-PPPD/pCKb11 also significantly suppressed the cancer progression. Our study demonstrated a nanotechnology-enabled delivery of pCKb11, that remodeled the immunosuppressive TME, for cancer treatment.

1. Introduction

As the most deadly gynecologic cancer, ovarian cancer is generally characterized by a high recurrence rate, poor prognosis, and high mortality rate [1]. Indeed, ovarian cancer is characterized by an immunosuppressive tumor microenvironment (TME), which strongly hinders anti-tumor immune responses and adversely affects the outcomes of immunotherapy [2]. Therefore, modulating and reversing the

immunosuppressive TME is a potential approach to treat ovarian cancer. Immunotherapy that activates anti-tumor immune responses is gradually developing as the most promising treatment strategy against malignancies [3]. However, immunotherapy-based “immune enhancement” strategies often induce severe immune-related adverse events [4]. In addition, unfavorable therapeutic responses attributed to the immunosuppressive TME also account for the low tumor response-to-toxicity profile of immunotherapy, which significantly

Peer review under responsibility of KeAi Communications Co., Ltd.

* Corresponding author.

E-mail address: xianggao@scu.edu.cn (X. Gao).

¹ These authors contributed equally to this work.

<https://doi.org/10.1016/j.bioactmat.2021.03.031>

Received 17 January 2021; Received in revised form 24 February 2021; Accepted 12 March 2021

2452-199X/© 2021 The Authors. Publishing services by Elsevier B.V. on behalf of KeAi Communications Co. Ltd. This is an open access article under the CC

BY-NC-ND license (<http://creativecommons.org/licenses/by-nc-nd/4.0/>).

restricts the clinical application of a majority of immunotherapies [5]. Recently, some important studies have revealed that the immune escape mechanisms produced by tumor cells caused a local rather than systematic immunosuppression, especially in solid tumors [6–8]. Thus, the strategies that target the activation of the anti-tumor immune response in TME will demonstrate relatively lower toxicity and better effects against tumors [5].

Among these recently developed immunotherapies, gene therapy-based immunotherapy (immunogene therapy) has shown superior effects. Immunogene therapy can stimulate anti-tumor immune responses by delivering and expressing foreign genes into target cells [9–11]. As the largest subfamily of cytokines, the chemoattractive and promotive traits of chemokines on various subtypes of leukocytes have garnered immense attention for improving the effects of immunotherapy by increasing the infiltration of immune cells in tumor tissues [12,13]. The C-C motif chemokine CKb11, also known as macrophage inflammatory protein-3 β , is constitutively expressed in lymphoid tissues and could chemoattract immunocytes [14]. The mechanisms underlying the effects mediated by CKb11 involve specific binding to its receptor C-C chemokine receptor 7 (CCR7), which is widely expressed in a variety of immune cells [15,16]. Moreover, CKb11 is necessary for the homing of T cells and dendritic cells (DCs) to lymphatic tissues, which could establish close interactions between T cells and DCs thus permitting antigen-specific activation [15]. Therefore, it is reasonable to hypothesize that the expression and secretion of CKb11 in tumor cells via gene therapy could lead to a locally high concentration of CKb11 in TME to attract and activate immune cells.

Gene delivery systems play a crucial role in the efficient delivery of foreign genes into target cells. Although both viral vectors and non-viral vectors have been employed in the delivery system for gene therapy, the use of viral vectors is still limited by the potential carcinogenicity, immunogenicity and limited DNA loading capacity [17,18]. Recent progress in nanotechnology has rendered nanoparticles excellent

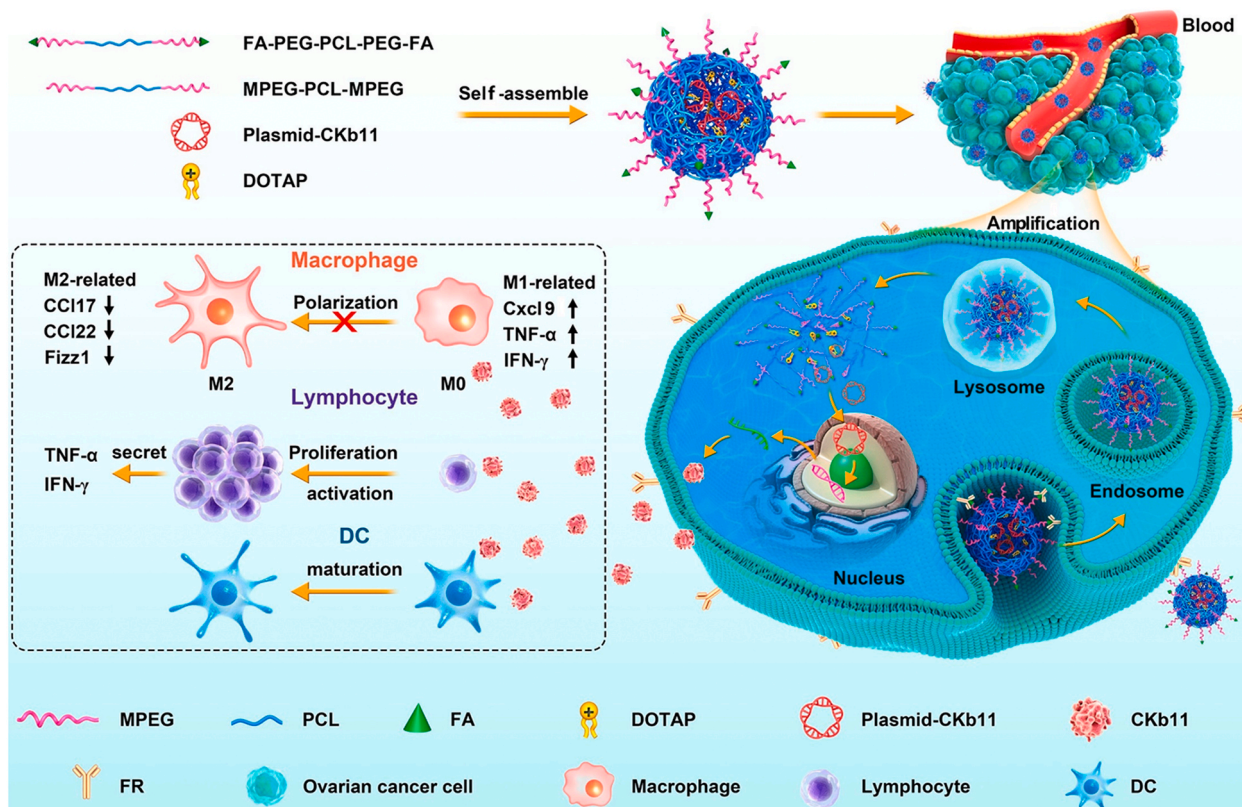
candidates for gene delivery carriers. However, the lack of tumor targeting and low transfection efficacy limit the application of nanoparticles. As a type of glycoproteins located on the cell surface, the folate receptor (FR) can bind to folic acid (FA) with high affinity and mediate the active uptake of FA [19]. In contrast to the extremely low expression level in most tissues, FR is overexpressed in various cancers, including ovarian cancer and breast cancer, to satisfy the FA requirement in fast-dividing cancer cells [20,21]. Thus, FA could be used as an excellent modifier for the targeted therapy of ovarian cancer, aiming to improve the tumor targeting of nanoparticles and reduce systemic toxicity.

In this study, we designed a tumor-targeting gene delivery system based on the self-assembly of FA-modified poly (ethylene glycol)-poly (ϵ -caprolactone)-poly (ethylene glycol) (FA-PEG-PCL-PEG-FA) and DOTAP to form FA-PEG-PCL-PEG-FA/DOTAP (F-PPPD) nanoparticles. The plasmid CKb11 (pCKb11) was encapsulated using F-PPPD nanoparticles to form the F-PPPD/pCKb11 complex. The study aimed to activate anti-tumor immune responses for treating ovarian cancer by employing the FA-modified non-viral vector-based delivery of pCKb11 (Scheme 1).

2. Materials and methods

2.1. Cells and animals

ID8 cells, a cell line that established from the spontaneously malignant transformation of ovarian surface epithelial cells (MOSEC) isolated from C57BL/6 mouse *in vitro*, were kindly provided by the State Key Laboratory of Biotherapy (SKLB). ID8 cells were cultured in Dulbecco's modified Eagle's medium (DMEM) (Gibco, USA), which supplemented with 10% fetal bovine serum (FBS), 100 U/mL of penicillin and 100 μ g/mL of streptomycin. The cells were maintained in a 37 °C incubator with humidity and 5% CO₂. C57BL/6 female mice (5–6 weeks old) were purchased from Beijing Huafukang Biotechnology Co. Ltd. (Beijing,



Scheme 1. Schematic representation of the process of immunogene therapy through the delivery of plasmid CKb11 (pCKb11) by F-PPPD nanoparticles.

China). In this study, all experiments about mice were conducted according to the guidelines approved by the Animal Experimental Ethics Committee of SKLB, Sichuan University.

2.2. Synthesis of MPEG-PCL-MPEG and FA-PEG-PCL-PEG-FA polymers

The MPEG-PCL-MPEG polymers were synthesized according to the following steps. MPEG (2000) (10.0 g) and ϵ -caprolactone (ϵ -CL) (10.0 g) were added to the flask under nitrogen flow, and maintained at 140 °C until complete melting. The Tin(II)2-ethylhexanoate was added as a catalyst for the ring-opening polymerization, and the reaction was allowed to proceed for 6–8 h. Next, hexamethylene diisocyanate (HMDI) was added to the mixture as a polymerizing agent and reacted for another 6–7 h. The crude product was dissolved in dichloromethane and precipitated by adding ice-cold petroleum ether, followed by filtration. After repeating the aforementioned step for thrice, the obtained product, MPEG-PCL-MPEG, was dialyzed and freeze-dried. Furthermore, FA-PEG-PCL-PEG-FA polymers were synthesized based on FA-PEG-PCL. Briefly, 200 mg of NH₂-PEG-PCL ($M_w = 5.1 \times 10^3$) and 100 mg of FA were dissolved in dimethyl sulfoxide (DMSO), followed by the addition of dicyclohexylcarbodiimide (DCC, 130 mg) and 4-dimethylaminopyridine (DMAP, 150 mg). After stirring at room temperature for 10 h, HMDI was added to this mixture and allowed to react for another 6–7 h. Finally, the crude product was dissolved in dichloromethane and precipitated by adding ice-cold petroleum ether, followed by filtration. After repeating the aforementioned step for thrice, the obtained product, FA-PEG-PCL-PEG-FA, was freeze-dried and stored at 4 °C.

2.3. Molecular dynamics of the interaction between FA-PEG-PCL-PEG-FA and DOTAP

The structure of DOTAP was first established with Marvin Sketch (<http://www.chemaxon.com>), followed by being refinement at the molecular mechanical level via the MMFF94 method [22]. The structure was further refined through the AM1 method with Fletcher-Reeves algorithm at a semi-empirical level using Hyperchem software (HyperChem, Professional 8.0) [23,24]. In addition, the structures of FA-PEG-PCL-PEG-FA were constructed and numerically simulated according to previously published methods [25]. The interactions between DOTAP and FA-PEG-PCL-PEG-FA were investigated in a water environment (pH = 7.0) and the environment near tumor tissue (pH = 6.7). The CHARMM27 was applied as the force field during the process [26]. Snapshots of the conformations of the FA-PEG-PCL-PEG-FA/DOTAP complex at 0 ns, 2 ns, 4 ns, 6 ns, 8 ns, and 10 ns were recorded and used to analyze the interactions.

2.4. Preparation of the F-PPPD/pCKb11 complex

Three ingredients, including 10 mg of DOTAP, 15 mg of FA-PEG-PCL-PEG-FA, and 75 mg of MPEG-PCL-MPEG were added to a round-bottom flask and melted with 2 mL acetone. Next, the acetone was evaporated from the mixture in a negative pressure environment using a water bath with a temperature of 55 °C for 20 min. Finally, 5% glucose solution (GS) (7.5 mL) was used to hydrate the product to generate the F-PPPD (2 mg/mL). Moreover, the MPEG-PCL-MPEG/DOTAP (named PPPD) (90% MPEG-PCL-MPEG and 10% DOTAP) nanoparticles were also synthesized with the same method. MPEG-PCL-MPEG, FA-PEG-PCL-PEG-FA and DOTAP self-assembled and formed a core-shell structure, namely F-PPPD. In detail, FA-PEG-PCL-PEG-FA micelles with an amphiphilic copolymer and amphiphilic cationic DOTAP were spontaneously assembled and folded into nanocomposites. The hydrophobic segment of FA-PEG-PCL-PEG-FA, generated from the hydrophobic PCL, contributed to the core structure. Meanwhile, the hydrophilic segment in the delivery system constructed a shell structure and maintained the stability of the drug-loading system. The pCKb11 or pvax was then added to this solution to obtain the F-PPPD/pCKb11 or F-PPPD/pvax complex via self-

assembly. The PPPD/pCKb11 complex was prepared using the same method. In this study, the pvax vector (Invitrogen, USA) was used as the control plasmid vector. The pCKb11 was established based on the pvax vector. All plasmid extractions in our study were processed using the EndoFree Plasmid Giga kit (Qiagen, Hilden, Germany).

2.5. Characterization of the F-PPPD/pCKb11 complex

Transmission electron microscopy (TEM, FEI Tecnai G2 F20, Hillsboro, OR, US) was used to analyze the morphological features of the F-PPPD/pCKb11 complex. Briefly, the samples were diluted with distilled water and placed on a copper grid. Before drying the grid, samples were negatively stained with phosphotungstic acid, then air-dried and examined using a TEM. The particle size and zeta-potential of the F-PPPD/pCKb11 complex were determined using the NanoBrook 90PLUS PALS particle size analyzer (Brookhaven Instruments, US).

2.6. Gel retardation assay

To detect the plasmids-loading capability of F-PPPD nanoparticles, agarose gel electrophoresis assay was performed. First, pCKb11 was added to the F-PPPD nanoparticles at different weight ratios (pCKb11:F-PPPD) of 1:0, 1:12.5, 1:25 and 1:50. Subsequently, these samples were subjected to electrophoresis in a 1% (w/v) agarose gel (Invitrogen, USA) in Tris-acetate-EDTA (TAE) buffer (pH 7.4; 120V, 20 min). The Gold View was served as a nucleic acid stain. Finally, the gel was photographed using a gel imaging system (Bio-Rad Laboratories, Hercules, CA, USA).

2.7. In vitro gene transfection efficiency

Since the green fluorescence protein (GFP) is the most frequently used reporter, the plasmids encoding enhanced GFP (pEGFP) were used as the reporting system for analyzing the transfection efficiency in our study. After seeding on the 6-well plate for 24 h, the medium of ID8 cells was replaced with the serum-free DMEM medium with 500 μ L per well. The nanoparticles (15 μ L) and pEGFP (5 μ g) were separately diluted in 250 μ L of the serum-free DMEM medium. The medium containing pEGFP was added to the medium containing nanoparticles and incubated for 20 min. Then, the ID8 cells were supplemented with the mixed medium for 4 h incubation. Subsequently, the medium was exchanging with the complete DMEM medium. After 48 h of culture, the transfected ID8 cells were observed under a fluorescent microscope (Olympus IX73, U-HPLGPS, Olympus Corporation, Tokyo, Japan). Moreover, the transfection efficiency was also measured by flow cytometry (ACEA Novo-Cyte™, ACEA Biosciences Inc., USA).

2.8. Intracellular trafficking

First, ID8 cells were pre-seeded in a dish with a glass bottom. The pCKb11 that labeled with green fluorescence dye YOYO-1 (YOYO™-1 Iodide (491/509), Invitrogen, USA) was encapsulated into F-PPPD nanoparticles, followed by being transfected into the ID8 cells. Next, the transfected ID8 cells were further stained with Lyso-tracker red probe and Hoechst 33342. Finally, the images of the stained ID8 cells were continuously captured under a confocal laser scanning microscopy (LSM880, ZEISS, Germany) for assessing the endosomal escape capability and intracellular localization of F-PPPD/pCKb11.

2.9. In vitro assays for immune cell stimulation and cytokine secretion

The ID8 cells were transfected with F-PPPD (vehicle), F-PPPD/pvax, PPPD/pCKb11, F-PPPD/pCKb11. The untreated cells were used as a negative control. After 48 h culture, the supernatants of the transfected tumor cells were collected and used to stimulate primary isolated lymphocytes, macrophages, and DCs, respectively. Primary murine spleen-

derived lymphocytes, bone marrow-derived macrophages and bone marrow-derived DCs were isolated according to previously described protocols [27–29]. After stimulation with the supernatants derived from transfected ID8 cells, lymphocytes were collected and stained with CD8, CD4, CD69, and IFN- γ to verify the activation of lymphocytes by flow cytometry. The macrophages were stained with CD45, CD11b, F4/80, and CD206 to observe the polarization status of macrophages, and the DCs were stained with CD11c, CD80, CD86 and MHCII for the detection of their maturation. All fluorescence-conjugated antibodies used for flow cytometry in this study were purchased from BD Biosciences (CA, USA) and Biolegend (USA), and the detailed information was supplied in the Supporting information. Furthermore, the supernatants derived from lymphocytes and macrophages, which have been stimulated by transfected tumor supernatants for 24 h, were collected to measure the secretion levels of TNF- α and IFN- γ by ELISA (Invitrogen, USA). The ELISA results were shown as the means of triplicate wells. Moreover, the proliferation of lymphocytes stimulated by supernatants derived from transfected tumor cells for 24 h was measured using the CCK-8 assay (Dojindo Molecular Technologies, Japan). Furthermore, supernatants derived from stimulated lymphocytes were collected and used to culture the ID8 cells for 24 h. The viability of ID8 cells was further evaluated using the CCK-8 assay.

2.10. Murine ovarian cancer model and treatment plan

An abdominal model of ovarian cancer was established in mice via intraperitoneal injection of ID8 cells (5×10^6 cells/mouse). After inoculation, mice were randomly allocated into five groups: (A) GS, 5% glucose solution; (B) F-PPPD nanoparticles (vehicle); (C) F-PPPD/pvax complex; (D) PPPD/pCKb11 complex; and (E) F-PPPD/pCKb11 complex. The treatments were initiated on the fourteenth day after inoculation. Briefly, the mice in the experimental group (F-PPPD/pCKb11 complex) were intraperitoneally injected with the complex of F-PPPD nanoparticles encapsulating pCKb11 (20 μ g per mouse) in 200 μ L of 5% GS. The mice in the other groups were injected with the same amounts of the corresponding nanoparticles and/or plasmids. The treatments were administered twice per week for a total of ten times. Furthermore, the body weights of mice were recorded every five days. Mice were euthanized on the 35th day after treatment. The tumor nodules, blood, ascites and vital organs of mice from each group were harvested. After being weighted, some tumor tissues were digested into single-cell suspensions for analyzing the TME through flow cytometry, and some tumor tissues and important visceral organs were lysed using RIPA lysis buffer to extract total proteins. The expression levels of CKb11 in the visceral organs were measured by ELISA (Abcam, USA). In addition, the expression levels of CKb11, TNF- α and IFN- γ in tumor tissues, ascites, and serum were also assessed using ELISA. Moreover, the survival of mice with the same grouping (ten mice per group) was recorded up to 90 days after the intraperitoneal inoculation with ID8 cells. The Kaplan–Meier curve was used to assess the survival of mice in each group.

2.11. Flow cytometry analysis of tumor-associated lymphocytes and macrophages in the peritoneal cavity

Mouse peritoneal lavage fluid was collected to analyze the phenotypes of tumor-associated lymphocytes and macrophages. Briefly, cold phosphate-buffered saline (PBS) was injected into the enterocoelia of mice with a gentle massage. The peritoneal wash fluid was collected, followed by lysing red blood cells (RBCs). To analyze the phenotype of lymphocytes in peritoneal cavity, the collected cells were stained with CD4, CD8, CD69, and IFN- γ and analyzed using flow cytometry. To analyze the polarization status of macrophages, the cells in peritoneal lavage fluid were stained with CD45, CD11b, F4/80 and CD206, and analyzed using flow cytometry.

2.12. Flow cytometry analysis of tumor-infiltrating immune cells

The tumor nodules from mice demonstrating abdominal metastasis model were collected, digested with collagenase IV (1 mg/mL) (Gibco, USA) and filtered through the cell strainer (BD Biosciences, CA, US) to obtain single-cell suspensions. These single-cell suspensions were stained with fluorescence-conjugated antibodies and analyzed using flow cytometry. The maturation of DCs was evaluated by staining with CD11c, CD80, CD86, and MHCII, and the natural killer (NK) cells were assessed by staining with CD49b and CD107a. Cells stained with CD3, CD4, and Foxp3 were used to assess the infiltration of regulatory T cells (T-regs). Furthermore, intratumoral infiltration of myeloid-derived suppressor cells (MDSCs) was analyzed by staining with CD11b and Gr1.

2.13. Immunohistochemical staining of CD31 and Ki-67

The tumor tissues from mice with abdominal metastasis were fixed with 4% paraformaldehyde, embedded in paraffin and then sectioned for immunohistochemical staining. The CD31 and Ki-67 were stained to evaluate the microvessel density (MVD) and tumor cell proliferation of the treated tumor tissues. The CD31-stained sections and Ki-67-stained sections were photographed under the optical microscope (Olympus, Japan). The number of CD31-positive vessels and the proportion of Ki-67-positive cells were analyzed in five randomized fields.

2.14. Terminal deoxynucleotidyl transferase dUTP nick end labeling (TUNEL) assay

To detect the in situ apoptosis of tumor tissues after treatments, the TUNEL assay was performed according to the manufacturer's instructions. After being stained, these sections were photographed under the fluorescence microscope (Olympus, Japan). The apoptotic cell was indicated by the colocalization of DAPI and green nucleus. The apoptotic index was counted and analyzed in five randomized fields.

2.15. Toxicity assessment

To evaluate the potential toxicity of F-PPPD/pCKb11 treatment, the histopathological assessment of important organs was conducted. These important organs, involving heart, liver, spleen, lung and kidney, were harvested from mice of each treatment group, fixed and embedded with paraffin wax. Then, these tissues were sectioned and stained with hematoxylin and eosin (H&E staining). The stained slices were observed and evaluated under the optical microscope (Olympus, Japan). Moreover, the blood samples of mice were also collected and used for routine blood tests. The remaining blood samples were placed at 4 $^{\circ}$ C for overnight, and then centrifuged to gain the serum samples. The serum samples were used to measure some important serological biochemical indicators via an automatic analyzer (Hitachi High-Technologies Corp., Japan).

2.16. Statistical analysis

Statistical analysis for comparing two groups was performed by Student's test, while One-way analysis of variance (ANOVA) was used for statistical analysis of multiple comparisons. Survival analysis was performed by the Kaplan–Meier method (Log-rank test). All statistical results were analyzed by using GraphPad Prism software version 7 (GraphPad, San Diego, US). All statistical values in this study were shown as a mean \pm standard error of measurement (SEM). The difference was considered to be statistically significant at p value < 0.05 (*p < 0.05 , **p < 0.01).

3. Results

3.1. Preparation and characteristics of F-PPPD/pCKb11

First, we evaluated the interactions between FA-PEG-PCL-PEG-FA and DOTAP in water environment (Fig. 1A and Fig. S1) and the environment near tumor tissue (Fig. 1B and Fig. S2) using molecular dynamics simulation. To achieve a suitable interaction site on the surface of FA-PEG-PCL-PEG-FA, the position and conformation of DOTAP were gradually altered. Meanwhile, FA-PEG-PCL-PEG-FA also coordinated its conformation dynamically until it produced a stable binding site for DOTAP. The conformation of DOTAP in the environment near tumor tissue (pH = 6.7) showed a minor change, while FA-PEG-PCL-PEG-FA showed an apparent change in its conformation. The interaction between FA-PEG-PCL-PEG-FA and DOTAP was weaker in the environment near tumor tissue with an energy of -36.27 kcal/mol, when compared with that in the water environment (-42.74 kcal/mol), which suggested a relatively easier release in the environment near tumor tissue. The ingredients MPEG-PCL-MPEG, FA-PEG-PCL-PEG-FA and DOTAP self-assembled and formed a core-shell structure, namely, F-PPPD. The structure model of F-PPPD/pCKb11 complexes was shown in Fig. 1C. On the surface of F-PPPD nanoparticles, the positive charge carried by the hydrophilic head of DOTAP could effectively attract plasmids by the interaction of static electricity. The spherical structure of F-PPPD/pCKb11 was identified using TEM (Fig. 1D). The mean diameter of F-PPPD/pCKb11 was 162.9 nm, with a zeta potential of -1.58 mV, demonstrating an approximately electroneutral feature of F-PPPD/pCKb11 complexes (Fig. 1E and F). Besides, the agarose gel electrophoresis assay was performed to detect the gene-loading capability of F-PPPD nanoparticles (Fig. 1G). The free plasmids appeared as a bright band (Lanes 1–3), and the cumulative retardation of plasmids was observed with mass ratios (pCKb11:F-PPPD) of 1:12.5 (lanes 4–6) and 1:25 (lanes 7–9). At a mass ratio of 1:50, no bright band was observed (lanes 10–12), indicating the complete encapsulation of pCKb11 by F-PPPD nanoparticles.

3.2. Intracellular distribution and transfection efficiency of F-PPPD/pCKb11 in tumor cells

Considering the importance of endosomal escape ability for gene carriers, we explored the intracellular distribution of F-PPPD/pCKb11 in ID8 cells. Continuous tracing (0.5, 2, 4.5, and 6 h) showed that the green fluorescence dye YOYO-1 labeled pCKb11 delivered by F-PPPD was initially co-located with endolysosomes, which labeled with Lyso-tracker (red) in the cytoplasm (Fig. S3A). Then, F-PPPD/pCKb11 gradually escaped from the endolysosomes and finally located into the nucleus. The overlay of the pCKb11 and nucleus in fluorescence intensities and positions manifested the endolysosomal escape ability of F-PPPD (Fig. S3B). High transfection efficiency is a prerequisite for effectual immunogene therapy. Next, we assessed the transfection efficiency of F-PPPD and PPPD in ID8 cells by transfecting with pEGFP-containing nanoparticles. The ID8 cells transfected with F-PPPD/pEGFP showed enhanced GFP expression compared to that in cells transfected with PPPD/pEGFP (Fig. 2A). The transfection efficiency was further detected by flow cytometry, showing significantly higher transfection efficiency for F-PPPD nanoparticles than that for PPPD nanoparticles (Fig. 2B). To effectively stimulate antitumor immune response, the pCKb11 was encapsulated into F-PPPD, and the efficiency of nanoparticles for CKb11 expression in the supernatants of ID8 cells was detected by ELISA. The pCKb11 delivered by F-PPPD improved the secretion of CKb11 compared with delivery by non-targeted PPPD nanoparticles (Fig. 2C). These results further demonstrated the potential of F-PPPD for gene delivery.

3.3. Delivery of pCKb11 in F-PPPD significantly promoted the activation of lymphocytes *in vitro*

Owing to the extensive expression of CCR7 in various subsets of immune cells including T cells, macrophages, and DCs, we next investigated the *in vitro* effects of F-PPPD/pCKb11 on these immune cells. The supernatants of transfected ID8 cells were collected and used to stimulate primary isolated lymphocytes, macrophages and DCs. Stimulation with supernatants derived from the F-PPPD/pCKb11 group significantly promoted the proliferation of lymphocytes (Fig. 3A). Subsequently, the supernatants derived from the stimulated lymphocytes were collected to culture fresh ID8 cells. The cell viability of ID8 cells was suppressed after incubation with supernatants of the lymphocytes from PPPD/pCKb11 and F-PPPD/pCKb11 groups, with the strongest inhibition demonstrated by the supernatants of the F-PPPD/pCKb11 group (Fig. 3B). As critically proinflammatory cytokines that are involved in mediating both innate and adaptive immune responses, TNF- α and IFN- γ are essential for tumor eradication [30,31]. The incubation of supernatants derived from ID8 cells transfected with PPPD/pCKb11 or F-PPPD/pCKb11 significantly increased the secretions of TNF- α and IFN- γ in lymphocytes, with the highest cytokine levels observed in the F-PPPD/pCKb11 groups (Fig. 3C and D). IFN- γ is primarily synthesized by activated CD4⁺ or CD8⁺ T lymphocytes, and CD69 typically works as a classical marker of lymphocyte activation [32]. Hence, the subset of activated lymphocytes was characterized by the positive expression of IFN- γ or CD69. After stimulation with the supernatants derived from transfected ID8 cells for 24 h, both PPPD/pCKb11 and F-PPPD/pCKb11 groups could effectively activate CD4⁺ and CD8⁺ T cells, while significantly higher proportions of IFN- γ ⁺ and CD69⁺ T cells were observed in the F-PPPD/pCKb11 group (Fig. 3E and F). Collectively, these results indicated the successfully secreted CKb11 protein from ID8 cells that was delivered by F-PPPD could effectively activate and promote the secretion of proinflammatory cytokines from T cells.

3.4. Delivery of pCKb11 in F-PPPD regulated the polarization of macrophages and maturation of DCs

As an essential component of innate immune cells, macrophages are recognized for two distinct polarization statuses, the classically activated M1 phenotype (pro-inflammatory) and alternatively activated M2 phenotype (immune-suppressive), according to the activation patterns and functions [33]. M1 macrophages tend to promote an anti-tumor immune response, while M2 macrophages exert tumor-promoting effects. Despite the tumor diversity, the M2-polarized macrophages with surface marker such as CD206, exhibit similar profiles that are associated with angiogenesis and suppression of anti-tumor immune responses [34]. Most tumor-associated macrophages (TAMs) exhibit an immunosuppressive M2 phenotype, which makes them good targets for cancer immunotherapy by driving the TAMs away from pro-tumoral phenotype towards anti-tumoral phenotype [35]. The supernatants derived from F-PPPD/pCKb11 transfected ID8 cells significantly inhibited the M2 polarization of macrophages and increased the proportion of M1-polarized macrophages, as indicated by the decreased proportion of F4/80⁺CD206⁺ cells (Fig. 4A). Next, we evaluated the expression levels of some representative genes associated with inflammatory or immunosuppressive polarization of macrophages using RT-PCR. After stimulation with the supernatants derived from F-PPPD/pCKb11 transfected ID8 cells, the expression levels of inflammation-related genes (NOS2, CXCL9, IL-6, IL-12 and IRF5) were significantly improved in macrophages. However, the expression levels of genes associated with immunosuppression (Fizz1, IL-10, IRF4, YM-1, CCL17 and CCL22) were obviously down-regulated (Fig. 4B). Furthermore, the stimulation with supernatants derived from F-PPPD/pCKb11 transfected ID8 cells also significantly increased the secretion of proinflammatory cytokines such as TNF- α and IFN- γ in macrophages (Fig. 4C and D). The activation of STAT1 plays a vital role in promoting M1 polarization in macrophages

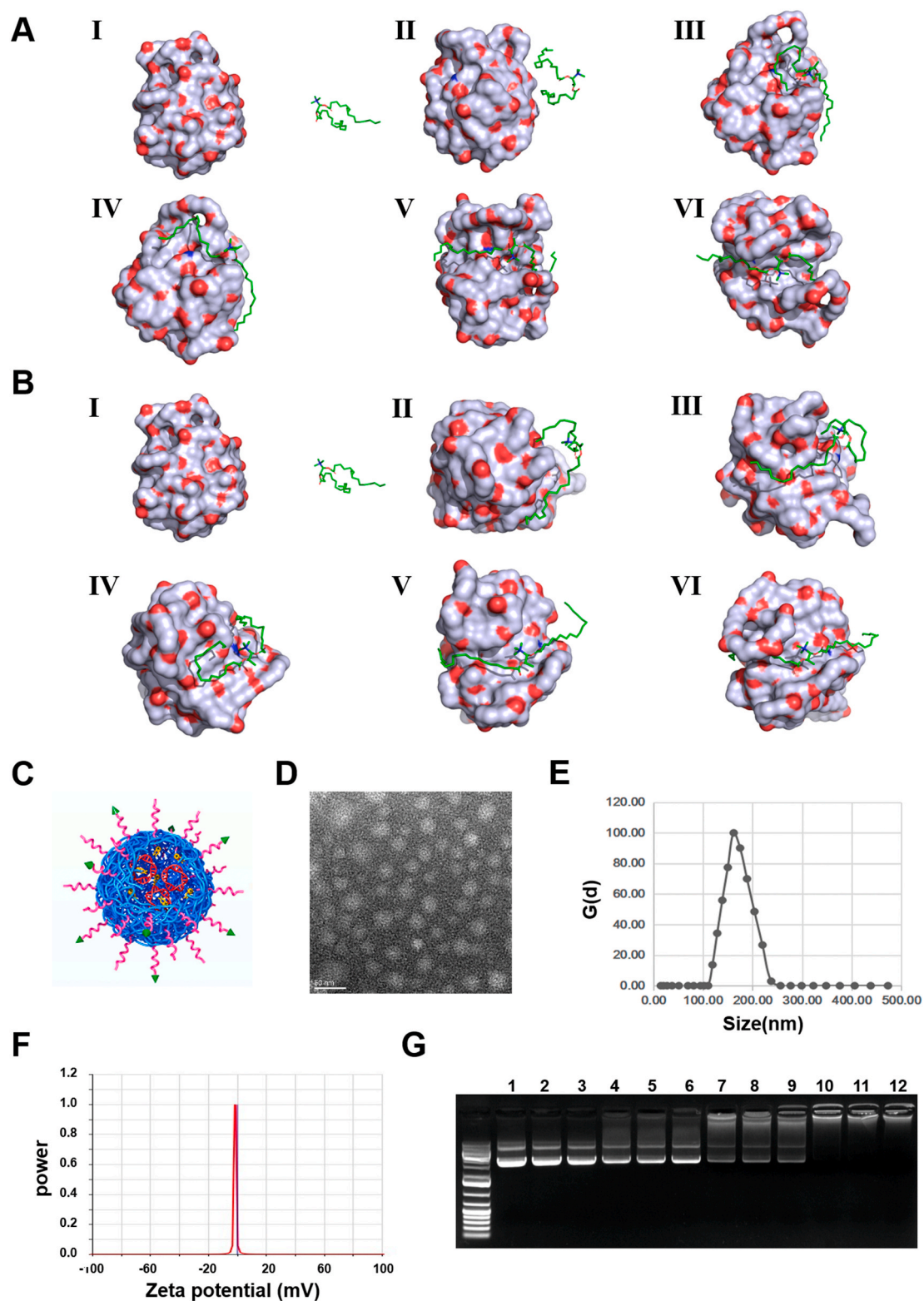


Fig. 1. Characterization of F-PPPD nanoparticles. The molecular dynamics simulation revealed the interaction modes between the DOTAP and copolymer in water environment (A) and environment near tumor tissue (B). The (I), (II), (III), (IV), (V) and (VI) were corresponded to the snapshots of conformations at 0 ns, 2 ns, 4 ns, 6 ns, 8 ns and 10 ns, respectively. (C) Structure model of F-PPPD/pCKb11 nanoparticles. (D) The TEM image of F-PPPD/pCKb11. (E) Size and (F) zeta potential of F-PPPD/pCKb11. (G) Agarose gel electrophoresis assay of the F-PPPD nanoparticles that loaded pCKb11. Lane 1–3, naked pCKb11; lanes 4–12, different mass ratios of pCKb11 with F-PPPD nanoparticles (lanes 4–6, 1:12.5; lanes 7–9, 1:25; lanes 10–12, 1:50).

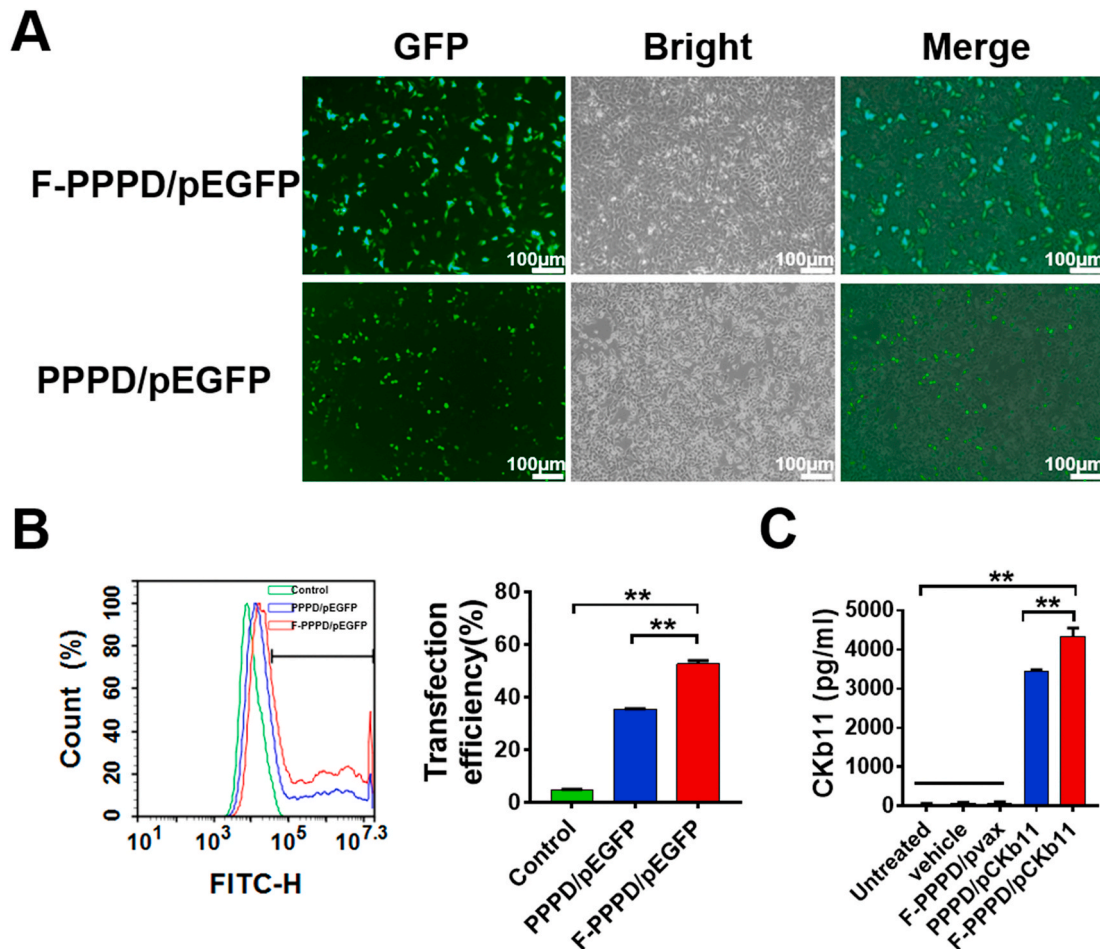


Fig. 2. Transfection efficiency of F-PPPD nanoparticles. (A) Representative images of GFP expression in transfected ID8 cells. (B) The transfection efficiency by flow cytometry. (C) The secretion level of CKb11 from ID8 cells by ELISA. (n = 3, **p < 0.01).

[36]. As shown in Fig. 4E, the STAT1 pathway was significantly activated in macrophages that stimulated by supernatants derived from F-PPPD/pCKb11 transfected ID8 cells, as indicated by increased protein levels of p-P65, p-STAT1, p-IRF3, IRF5, iNOS, and decreased protein levels of IRF4 and YM-1. In summary, these results suggested that CKb11 secreted from ID8 cells after the delivery of F-PPPD could effectively promote M1 polarization of macrophages by activating the STAT1 pathway (Fig. 4F).

DCs play a critical role in anti-tumor immune responses through processing and presenting tumor antigens to T cells. Thus, we further assessed the maturation of DCs by measuring the expressions of costimulatory molecules CD80, CD86, and MHCII. The supernatants derived from F-PPPD/pCKb11 transfected ID8 cells significantly increased the maturation of DCs, and that in PPPD/CKb11 group was slightly increased (Fig. 5). Taken together, these results collectively suggested the pCKb11 delivered by F-PPPD could effectively stimulate these crucial immune cells *in vitro*, manifested as activating T cells, inhibiting the M2 polarization of macrophages and inducing the maturation of DCs.

3.5. Administration of F-PPPD/pCKb11 significantly suppressed the intraperitoneal progression of ovarian cancer

Next, we evaluated whether F-PPPD/pCKb11 treatment could effectively suppress the intraperitoneal growth of ovarian cancer. When compared to treatment with GS, vehicle, or F-PPPD/pvax, treatment with PPPD/pCKb11 or F-PPPD/pCKb11 significantly inhibited the tumor growth in murine model of ovarian cancer (Fig. 6A–C). The

average tumor weight and ascites volume were remarkably reduced in both PPPD/pCKb11 and F-PPPD/pCKb11 treatment groups, without any apparent changes in the body weight (Fig. 6D–F). Moreover, a significantly potent anti-tumor effect and prolonged overall survival were observed in the F-PPPD/pCKb11 treatment group than those in PPPD/pCKb11 treatment group (Fig. 6G). Therefore, pCKb11 delivered by F-PPPD nanoparticles demonstrated the highest efficiency in inhibiting the intraperitoneal progression of ovarian cancer. Furthermore, the tumor vessels were assessed by CD31 staining and the proliferation of tumor cells *in vivo* was evaluated by Ki-67 staining. As shown in Fig. 6H and I, the F-PPPD/pCKb11 treatment demonstrated the strongest anti-angiogenic and anti-proliferative effects. To explore whether F-PPPD/pCKb11 treatment caused tumor suppression was associated with apoptosis, the TUNEL assay was used to detect the intratumoral apoptosis. Treatment with F-PPPD/pCKb11 led to a significant increase in the proportion of apoptotic cells, whereas other treatments showed only a few apoptotic cells in the tumors (Fig. 6J). These results implied that decreased tumor angiogenesis, suppressed tumor cell proliferation and increased intratumoral apoptosis might be the result of significantly enhanced intratumoral anti-tumor immunity obtained by treatment with F-PPPD/pCKb11.

3.6. Administration of F-PPPD/pCKb11 significantly reshaped the immunosuppressive TME

The immunosuppressive TME has been identified as the major cause of the inadequate response of immunotherapy in ovarian cancer. Accordingly, we further assessed whether the improved anti-tumor

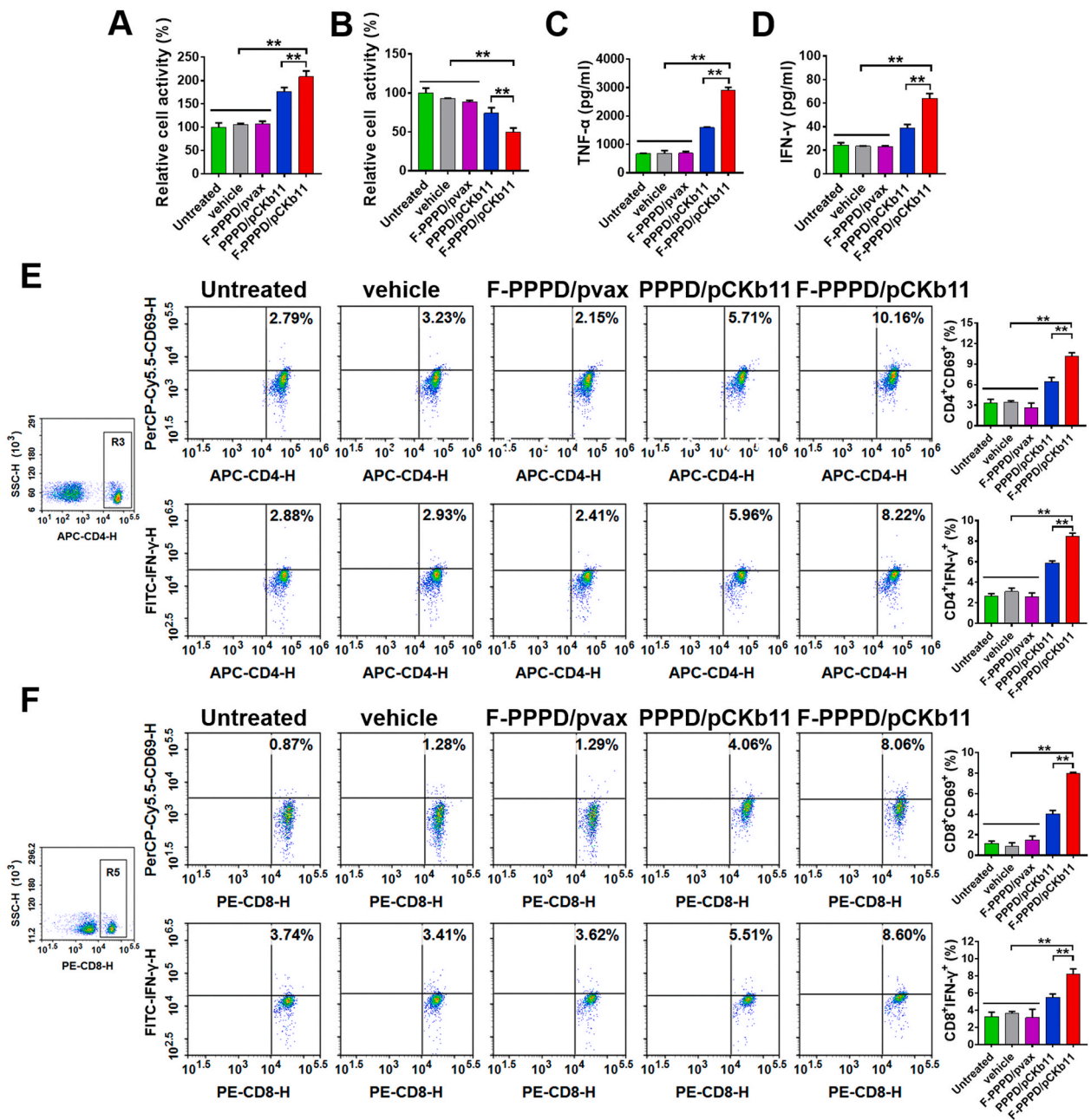


Fig. 3. Activation of lymphocytes *in vitro*. (A) Proliferation activity of lymphocytes by CCK-8. (B) The supernatants from stimulated lymphocytes were used to culture ID8 cells for 24 h, and then the cell viability of ID8 cells was measured by CCK-8. After being stimulated by the supernatants from different transfected ID8 cells, the secretion levels of TNF- α (C) and IFN- γ (D) from lymphocytes were measured by ELISA, and the subsets of activated CD4⁺ (E) and CD8⁺ (F) lymphocytes were measured by flow cytometry. (n = 3, **p < 0.01).

effect was based on the reshaping of the immunosuppressive TME. The administration of F-PPPD/pCKb11 significantly increased the secretion of CKb11 at tumor sites and ascites in the ovarian cancer model (Fig. 7A). Moreover, the secretions of pro-inflammatory cytokines, such as IFN- γ and TNF- α were obviously up-regulated after the treatment with PPPD/pCKb11, which were further increased upon treatment with F-PPPD/pCKb11 (Fig. 7A). Besides, no changes in the expression levels of CKb11, IFN- γ and TNF- α were observed in serums obtained from each treatment group, which indicated locally high concentrations of immunostimulatory CKb11 and cytokines such as IFN- γ and TNF- α in tumor tissues with inapparent systemic inflammatory response (Fig. 7A). Furthermore, CKb11 expression levels in the visceral organs were also measured (Fig. 7B). No significant difference in CKb11 expression was detected in organs such as the heart, liver, lung and

kidney after different treatments, which further demonstrated the tumor-targeting ability of F-PPPD. The slight increase of CKb11 expression was found in the spleen, which might be caused by an activated immune response of lymphocytes after treatment with PPPD/pCKb11 or F-PPPD/pCKb11.

We next examined the influence of CKb11 based immunogene therapy on the infiltration of immune cells in the TME. Treatment with PPPD/pCKb11 or F-PPPD/pCKb11 significantly increased the intratumoral infiltration of activated CD4⁺ and CD8⁺ T cells, as indicated by increased expressions of CD69 and IFN- γ (Fig. S4 and S5). In addition, treatment with F-PPPD/pCKb11 resulted in a substantial decrease in the proportion of the M2 macrophages in peritoneal fluid, with an increased M1/M2 ratio (Figure S6). The tumor-associated antigens presented by antigen-presenting cells (APCs), especially intratumoral DCs, are

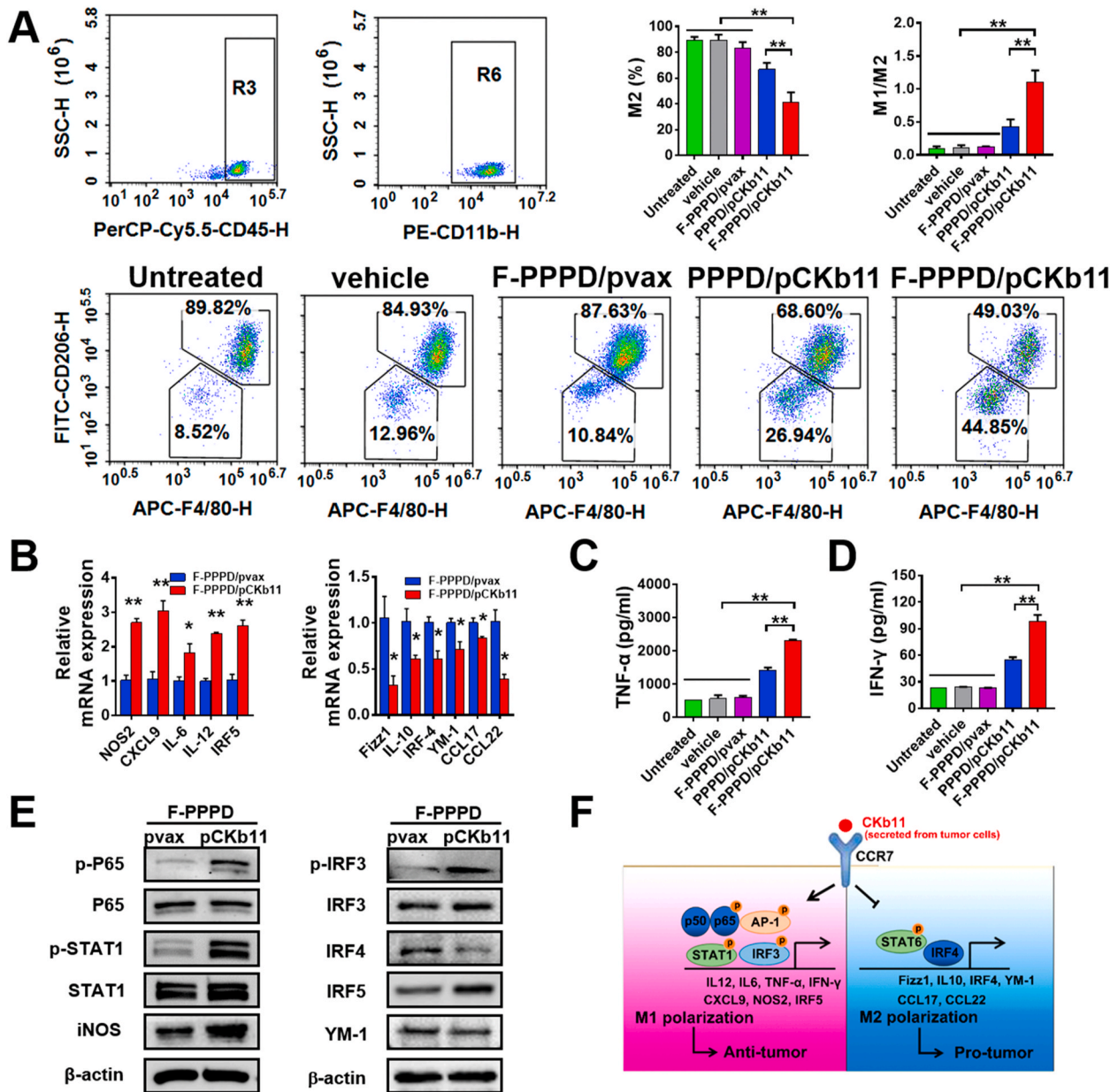


Fig. 4. Polarization of macrophages *in vitro*. (A) After being stimulated by the supernatants from transfected ID8 cells for 24 h, the polarization status of macrophages *in vitro* was analyzed by flow cytometry. (B) The mRNA levels of inflammation-related genes (left) and immunosuppression-related genes (right) in stimulated macrophages were detected by RT-PCR. The secretion levels of TNF- α (C) and IFN- γ (D) from stimulated macrophages were measured by ELISA. (E) Protein levels were detected in the macrophages stimulated by supernatants from F-PPPD/pvax or F-PPPD/pCKb11 transfected ID8 cells. (F) Brief illustration of the mechanism that CKb11 induced polarization of macrophages. (n = 3, *p < 0.05; **p < 0.01).

frequently linked with the priming of cytotoxic T cells in the TME. Hence, we next examined whether F-PPPD/pCKb11 treatment could trigger the maturation of tumor-infiltrating DCs by flow cytometry. Treatment with PPPD/pCKb11 or F-PPPD/pCKb11 resulted in up-regulating expressions of DCs maturation markers, CD80, CD86, and MHCII, in CD11c⁺ tumor-infiltrating DCs (Fig. S7). The NK cells can not only kill tumor cells directly, but also secrete various cytokines, chemokines, and growth factors to activate other immune cells [37]. The intratumoral infiltration of NK cells is associated with better prognosis [38]. Treatment with F-PPPD/pCKb11 showed the strongest effect on promoting the infiltration of NK cells in tumor tissues, as indicated by increased expressions of CD49b and CD107a (Fig. S8).

The recruitment of immunosuppressive cell populations including T-regs and MDSCs has been specially concerned for resulting in immune suppression in TME [39,40]. Therefore, we next examined whether the

delivery of pCKb11 by nanoparticles could effectively remodel the immunosuppressive TME in ovarian cancer. Administration of PPPD/pCKb11 to mice bearing ovarian cancer significantly suppressed the infiltration of T-regs, with a further reduction of the infiltration observed in F-PPPD/pCKb11 treated group (Fig. S9). Furthermore, compared with the PPPD/pCKb11 treatment, administration of F-PPPD/pCKb11 significantly reduced the intratumoral infiltration of MDSCs (Fig. S10). Collectively, these results collectively suggested the mechanism of the potent anti-tumor effects exerted by F-PPPD/pCKb11 might be involved in enhancing the anti-tumor immunity, as indicated by chemoattracting and activating T cells, suppressing the M2 polarization of macrophages, promoting the maturation of DCs, facilitating the infiltration of NK cells to tumor sites, as well as inhibiting the intratumoral infiltration of immunosuppressive T-regs and MDSCs.

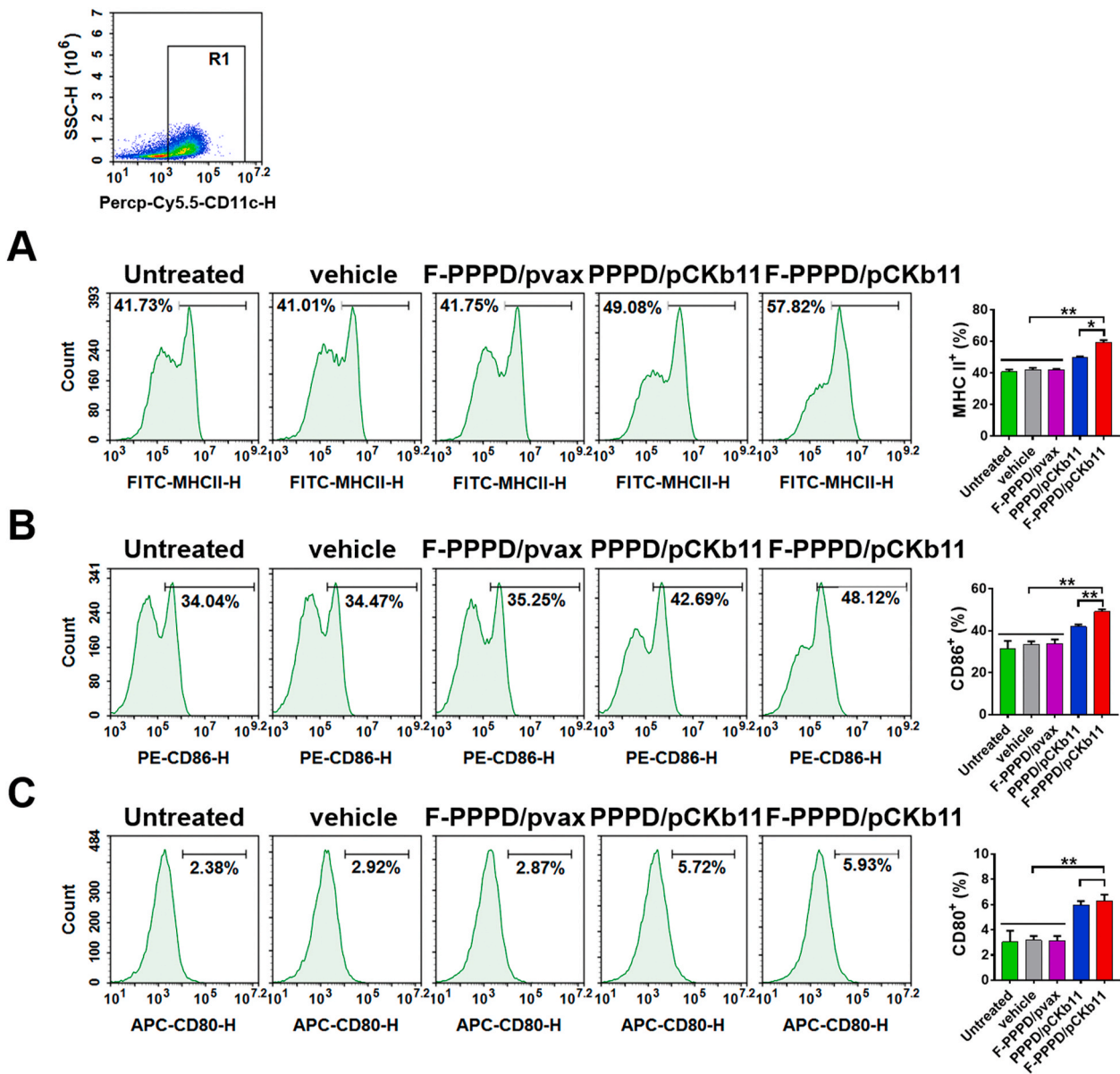


Fig. 5. Maturation of DCs *in vitro*. After being stimulated by the supernatants from transfected ID8 cells for 24 h, the percentages of matured DCs *in vitro* were analyzed by flow cytometry. (n = 3, *p < 0.05; **p < 0.01).

3.7. Safety assessment of F-PPPD/pCk11 treatment

The safety of F-PPPD/pCk11 treatment in mice with ovarian cancer was assessed. First, no abnormally histopathological changes, including necrosis, lesions or inflammation, were observed in the H&E staining of vital organs obtained from mice after treatment (Fig. S11). The F-PPPD/pCk11 treatment was well tolerated by mice, as indicated by the non-significant changes in hepatic function indices, renal function indices and blood lipid indices (Fig. S12). Moreover, routine blood tests showed no hematological changes (Fig. S13). In summary, the preliminary safety evaluation demonstrated that this immunogene therapy of pCk11 delivered by F-PPPD nanoparticles was well tolerated in mice without systemic toxicity.

4. Discussion

The effective infiltration and activation of immune cells in tumor tissues are the basis and prerequisite for effective tumor immunotherapy [41]. Therefore, modulating the distribution and activation status of

immune cells to enhance anti-tumor immune responses is promising for tumor immunotherapy. As the largest subfamily of cytokines, the chemoattractive and promotive traits of chemokines on various subtypes of leukocytes have garnered immense attention for enhancing the effects of immunotherapy by increasing the infiltration of immune cells in tumor tissues [13]. Thereinto, chemokine Ck11 has been reported to attract and activate T cells, which suggested its potential as a candidate for immune cell recruitment and activation-based tumor immunotherapy. Herein, this study was designed to investigate the efficiency of nanoscale immunogene therapy.

The first use of cytokines in tumor immunotherapy was demonstrated more than 30 years ago. However, most cytokine-based immunotherapy trials have not acquired anticipated effects. The major obstacle of cytokine-based immunotherapy is to determine a therapeutically relevant dosage that does not demonstrate excessive adverse toxicity in patients [12]. The recombinant cytokines used in clinical trials have been observed for rapid clearance and short plasma half-life, which significantly attenuates the anti-tumor efficiency [42,43]. Moreover, the parenteral administration of cytokines at high dose to reach

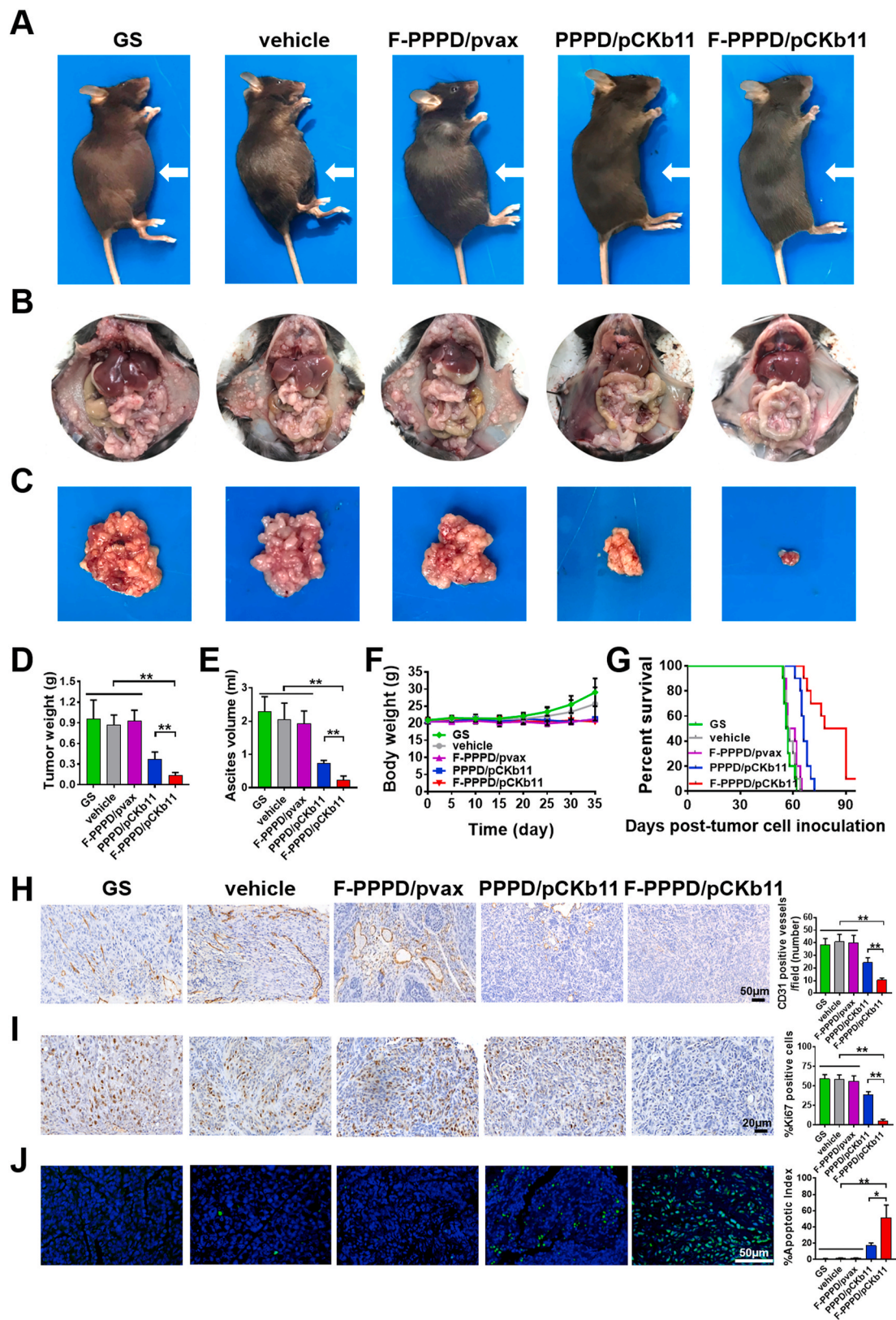


Fig. 6. Anticancer effect of F-PPPD/pCk11 in the peritoneal ovarian cancer model. The appearance of mice (A), representative images of the peritoneal cavity of mice (B) and corresponding tumors (C). (D) Tumor weights and (E) ascites volume of mice in different groups (n = 10). (F) Body weight curves. (G) Overall survival curves (n = 10). Representative images of the CD31 (H), Ki-67 (I) and TUNEL (J) staining of tumor tissues. (*p < 0.05; **p < 0.01).

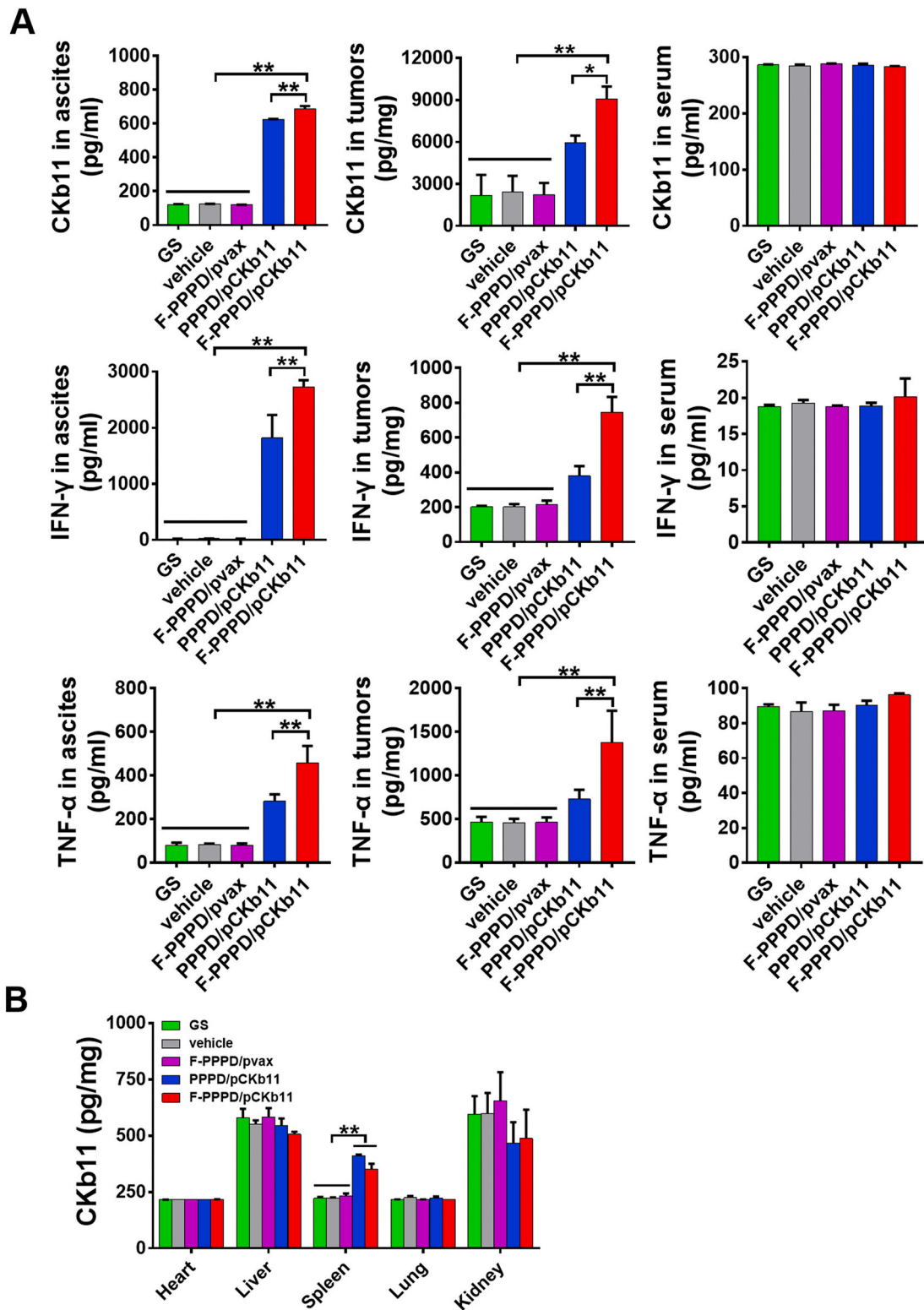


Fig. 7. F-PPPD/pCKb11 treatment increased CKb11, IFN-γ and TNF-α expressions in peritoneal ovarian cancer model. (A) Ascites, tumor tissue and serum were collected after different treatments with GS, F-PPPD, F-PPPD/pvax, PPPD/pCKb11 and F-PPPD/pCKb11, and the expressions of CKb11, IFN-γ and TNF-α by ELISA in the ascites, tumor tissues, and serum were measured. (B) In addition, the expressions of CKb11 in visceral organs (heart, liver, spleen, lung, kidney) were also detected by ELISA. (n = 5; *p < 0.05, **p < 0.01).

therapeutically effective concentrations in tumor tissues often induces severe systemic toxicities [44]. The application of novel gene therapy approaches has remarkably promoted the prospects of chemokine-based immunotherapy. The delivery system used in chemokine-based

immunotherapy should be designed with improved transfection efficiency, tumor-specific uptake and stable expression of chemokines, effectively inducing the infiltration and activation of immune cells in tumor tissues [45]. Although both viral vectors and non-viral vectors

have been employed in the delivery system of gene therapy, the use of viral vectors is still limited by their potential carcinogenicity, immunogenicity and limited DNA loading capacity [17,18]. Thus, non-viral nanoparticles with relative safety, high transfection efficiency and low immunogenicity were synthesized in this study for the delivery of pCKb11. Based on the previous findings showing significantly higher expression of FR in ovarian cancer cells than that in normal tissues, we utilized FR as the target to improve the tumor-specific uptake of plasmids [20]. In the present study, the modification of FA in F-PPPD nanoparticles significantly increased the transfection efficiency, generated more plasmids uptake in ovarian cancers, and induced higher expression of CKb11 proteins when compared with the effects observed with PPPD nanoparticles. Moreover, the locally high concentration of CKb11 at tumor sites and minor changes in visceral organs also suggested excellent tumor-targeting ability and high transfection efficiency of F-PPPD plasmids *in vivo*. Therefore, the F-PPPD nanoparticles demonstrated the potential to be served as a reliable gene delivery carrier.

In this study, the administration of F-PPPD/pCKb11 not only significantly suppressed the abdominal metastasis of ovarian cancer, but also obviously prolonged the overall survival of mice. The mechanism of the excellent anti-tumor activity induced by F-PPPD/pCKb11 treatment might be involved in enhanced anti-tumor immunity, as indicated by chemoattracting and activating T cells, promoting the maturation of DCs, suppressing the M2 polarization of macrophages, facilitating the infiltration of NK cells to tumor sites, as well as inhibiting the infiltration of immunosuppressive T-regs and MDSCs. Inducing the maturation of intratumoral DCs that are required for the priming of naive T cells and T cell-mediated anti-cancer immunity might be an effective anti-tumor strategy [46]. Our results showed the treatment with F-PPPD/pCKb11 significantly increased the expressions of costimulatory molecules CD80, CD86 and MHCII both *in vitro* and in intratumoral DCs, suggesting elevated DCs maturation. In addition, treatment with F-PPPD/pCKb11 also activated T cells and stimulated the secretions of IFN- γ and TNF- α , which are essential for tumor eradication. Another important effect of F-PPPD/pCKb11 treatment was suppressing the M2 polarization of tumor-infiltrating macrophages, which resulted in the polarization of macrophages toward an antitumoral phenotype. Most TAMs exhibit an immunosuppressive M2 phenotype, which makes them good targets for cancer immunotherapy that acts by driving the TAMs away from the pro-tumoral phenotype towards the anti-tumoral phenotype [35]. More importantly, FA-targeted vectors are easily cleared by M2 macrophages because the expression of FR- β and uptake of FA are characteristic features of M2 macrophages [47]. FA functionalization leads to the aggravated capture of liposomes by M2 macrophages *in vivo* [47]. Our research confirmed the CKb11 led to the suppression of macrophage M2 polarization, which could solve the problem of phagocytosis of FA by macrophages. Furthermore, the intratumoral infiltration of immunosuppressive cell populations including T-regs and MDSCs, was also decreased after treatment with F-PPPD/pCKb11. The significantly increased tumor apoptosis in F-PPPD/pCKb11-treated mice was the result of a significantly enhanced anti-tumor immune response mediated by the delivery of pCKb11. Moreover, the tumor-targeted delivery of pCKb11 with F-PPPD was well tolerated in mice without systemic toxicity.

Compared with current immunotherapies, the strategy used in this study has some superiorities. The delivery of pCKb11 by F-PPPD nanoparticles resulted in the successful production of CKb11 with biological activity by tumor cells. The parenteral administration of cytokines at high dose to reach therapeutically effective concentrations in tumor tissues often induces severe systemic toxicities [12,44]. Our study established a locally high concentration of CKb11 in the TME to attract and activate immune cells, which has the potential to avoid the adverse effects of systemic administration of CKb11 protein. Furthermore, the *in vivo* administration of recombinant proteins that lack proper glycosylation might induce the production of neutralizing antibodies, thereby

reducing the anti-tumor efficiency [48]. In addition, the targeted delivery system used in our study is superior to other reported tumor targeting gene delivery systems. First, the drawbacks of cationic lipids include toxicity, relatively inefficient, and non-specific delivery [49]. Second, polyethylene imines (PEIs) are toxic. Although the toxicity decreases for smaller or linear PEIs, transfection efficiency is also degraded [50]. Third, inorganic nanoparticles such as gold nanoparticles and silica nanoparticles have toxicity, and exhibit solubility limitations [51]. In contrast, the tumor-targeting gene delivery system used in our study were safe and easy to prepare, with low immunogenicity and less systemic toxicity, and the transfection efficiency was further improved by modification with FA.

5. Conclusions

In summary, the novel and FA-modified nanoparticle-enabled delivery of pCKb11 was highly efficient and safe, which successfully chemoattracted and activated T cells, suppressed M2 polarization and promoted M1 polarization of macrophages, increased the maturation of DCs, facilitated the intratumoral infiltration of NK cells, and inhibited the infiltration of immunosuppressive cells in ovarian cancer. The F-PPPD-delivered pCKb11 was confirmed to be safe and well-tolerated in mice without systemic toxicity, indicating that F-PPPD nanoparticles might be served as a reliable gene delivery carrier. Compared with current immunotherapies, this strategy exhibits significant potential for application as novel immune cell recruitment and activation-based cancer immunotherapy in the future.

CRedit authorship contribution statement

Wen Nie: Investigation, Methodology, Writing – original draft. **Ting Yu:** Investigation, Methodology, Writing – original draft. **Xiaoxiao Liu:** Investigation, Methodology, Validation. **Bilan Wang:** Formal analysis. **Tingting Li:** Data curation. **Yin Wu:** Data curation. **Xikun Zhou:** Writing – review & editing. **Lu Ma:** Writing – review & editing. **Yunfeng Lin:** Writing – review & editing. **Zhiyong Qian:** Writing – review & editing. **Xiang Gao:** Conceptualization, Methodology, Supervision, Writing – review & editing.

Declaration of competing interest

The authors declare that they have no known competing financial interests or personal relationships that could have appeared to influence the work reported in this paper.

Acknowledgements

This work was supported by the Ministry of Science and Technology of the People's Republic of China (No. 2018ZX09201018). This work was supported by Sichuan Science and Technology Program (No. 2019YFS0089, 2019YFS0340 and 2020YFS0217). This work was supported by the China Postdoctoral Science Foundation (No. 2020M680150) and full-time postdoctoral research and development fund of Sichuan University (No. 20826041D4048). This work was supported by the full-time postdoctoral research and development fund of West China Hospital of Sichuan University (No. 2020HXBH059 and No. 2020HXBH002), 1-3-5 project of excellent development of discipline of West China Hospital of Sichuan University (No. ZYYC21005), and the Natural Science Foundation Youth Project of Jiangsu Province (BK20190989).

Appendix A. Supplementary data

Supplementary data to this article can be found online at <https://doi.org/10.1016/j.bioactmat.2021.03.031>.

References

- [1] R.L. Siegel, K.D. Miller, A. Jemal, Cancer statistics, *CA A Cancer J. Clin.* 70 (1) (2020) 7–30, 2020.
- [2] C. Chester, O. Dorigo, J.S. Berek, H. Kohrt, Immunotherapeutic approaches to ovarian cancer treatment, *J Immunother Cancer* 3 (2015) 7.
- [3] I. Mellman, G. Coukos, G. Dranoff, Cancer immunotherapy comes of age, *Nature* 480 (7378) (2011) 480–489.
- [4] D.J. Schwartzentruber, D.H. Lawson, J.M. Richards, R.M. Conry, D.M. Miller, J. Treisman, F. Gailani, L. Riley, K. Conlon, B. Pockaj, K.L. Kendra, R.L. White, R. Gonzalez, T.M. Kuzel, B. Curti, P.D. Leming, E.D. Whitman, J. Balkissoon, D. S. Reintgen, H. Kaufman, F.M. Marincola, M.J. Merino, S.A. Rosenberg, P. Choyke, D. Vena, P. Hwu, gp100 peptide vaccine and interleukin-2 in patients with advanced melanoma, *N. Engl. J. Med.* 364 (22) (2011) 2119–2127.
- [5] M.F. Sanmamed, L. Chen, A paradigm shift in cancer immunotherapy: from enhancement to normalization, *Clin. Cells* 175 (2) (2018) 313–326.
- [6] I. Melero, G. Gaudernack, W. Gerritsen, C. Huber, G. Parmiani, S. Scholl, N. Thatcher, J. Wagstaff, C. Zielinski, I. Faulkner, H. Mellstedt, Therapeutic vaccines for cancer: an overview of clinical trials, *Nat. Rev. Clin. Oncol.* 11 (9) (2014) 509–524.
- [7] J.M. Taube, R.A. Anders, G.D. Young, H. Xu, R. Sharma, T.L. McMiller, S. Chen, A. P. Klein, D.M. Pardoll, S.L. Topalian, L. Chen, Colocalization of inflammatory response with B7-h1 expression in human melanocytic lesions supports an adaptive resistance mechanism of immune escape, *Sci. Transl. Med.* 4 (127) (2012) 127ra37.
- [8] L. Chen, X. Han, Anti-PD-1/PD-L1 therapy of human cancer: past, present, and future, *J. Clin. Invest.* 125 (9) (2015) 3384–3391.
- [9] L. Cheng, X. Du, Z. Wang, J. Ju, M. Jia, Q. Huang, Q. Xing, M. Xu, Y. Tan, M. Liu, P. Du, L. Su, S. Wang, Hyper-IL-15 suppresses metastatic and autochthonous liver cancer by promoting tumour-specific CD8+ T cell responses, *J. Hepatol.* 61 (6) (2014) 1297–1303.
- [10] G. Zhu, L. Mei, H.D. Vishwasrao, O. Jacobson, Z. Wang, Y. Liu, B.C. Yung, X. Fu, A. Jin, G. Niu, Q. Wang, F. Zhang, H. Shroff, X. Chen, Intertwining DNA-RNA nanocapsules loaded with tumor neoantigens as synergistic nanovaccines for cancer immunotherapy, *Nat. Commun.* 8 (1) (2017) 1482.
- [11] K.W. Huang, F.F. Hsu, J.T. Qiu, G.J. Chern, Y.A. Lee, C.C. Chang, Y.T. Huang, Y. C. Sung, C.C. Chiang, R.L. Huang, C.C. Lin, T.K. Dinh, H.C. Huang, Y.C. Shih, D. Alson, C.Y. Lin, Y.C. Lin, P.C. Chang, S.Y. Lin, Y. Chen, Highly efficient and tumor-selective nanoparticles for dual-targeted immunogene therapy against cancer, *Sci Adv* 6 (3) (2020), eaax5032.
- [12] B. Homey, A. Muller, A. Zlotnik, Chemokines: agents for the immunotherapy of cancer? *Nat. Rev. Immunol.* 2 (3) (2002) 175–184.
- [13] F. Sallusto, M. Baggiolini, Chemokines and leukocyte traffic, *Nat. Immunol.* 9 (9) (2008) 949–952.
- [14] A. Rot, U.H. von Andrian, Chemokines in innate and adaptive host defense: basic chemokines grammar for immune cells, *Annu. Rev. Immunol.* 22 (2004) 891–928.
- [15] R. Forster, A.C. Davalos-Misslitz, A. Rot, CCR7 and its ligands: balancing immunity and tolerance, *Nat. Rev. Immunol.* 8 (5) (2008) 362–371.
- [16] B.J. Marsland, P. Battig, M. Bauer, C. Ruedl, U. Lassing, R.R. Beerli, K. Dietmeier, L. Ivanova, T. Pfister, L. Vogt, H. Nakano, C. Nembrini, P. Saudan, M. Kopf, M. F. Bachmann, CCL19 and CCL21 induce a potent proinflammatory differentiation program in licensed dendritic cells, *Immunity* 22 (4) (2005) 493–505.
- [17] C. Baum, O. Kustikova, U. Modlich, Z. Li, B. Fehse, Mutagenesis and oncogenesis by chromosomal insertion of gene transfer vectors, *Hum. Gene Ther.* 17 (3) (2006) 253–263.
- [18] N. Bessis, F.J. GarciaCozar, M.C. Boissier, Immune responses to gene therapy vectors: influence on vector function and effector mechanisms, *Gene Ther.* 11 (Suppl 1) (2004) S10–S17.
- [19] C. Chen, J. Ke, X.E. Zhou, W. Yi, J.S. Brunzelle, J. Li, E.L. Yong, H.E. Xu, K. Melcher, Structural basis for molecular recognition of folic acid by folate receptors, *Nature* 500 (7463) (2013) 486–489.
- [20] M. Kobel, J. Madore, S.J. Ramus, B.A. Clarke, P.D. Pharoah, S. Deen, D.D. Bowtell, K. Odunsi, U. Menon, C. Morrison, S. Lele, W. Bshara, L. Sucheston, M. W. Beckmann, A. Hein, F.C. Thiel, A. Hartmann, D.L. Wachter, M.S. Anglesio, E. Hogdall, A. Jensen, C. Hogdall, K.R. Kalli, B.L. Fridley, G.L. Keeney, Z. C. Fogarty, R.A. Vierkant, S. Liu, S. Cho, G. Nelson, P. Ghatage, A. Gentry-Maharaj, S.A. Gayther, E. Benjamin, M. Widschwendter, M.P. Interaggio, B. Rosen, M. Q. Bernardini, H. Mackay, A. Oza, P. Shaw, M. Jimenez-Linan, K.E. Driver, J. Alsop, M. Mack, J.M. Koziak, H. Steed, C. Ewanowich, A. DeFazio, G. Chenevix-Trench, S. Feraday, B. Gao, S.E. Johnatty, J. George, L. Galletta, A.S. Group, E.L. Goode, S. K. Kjaer, D.G. Huntsman, P.A. Fasching, K.B. Moysich, J.D. Brenton, L.E. Kelemen, Evidence for a time-dependent association between FOLR1 expression and survival from ovarian carcinoma: implications for clinical testing. An Ovarian Tumour Tissue Analysis consortium study, *Br. J. Cancer* 111 (12) (2014) 2297–2307.
- [21] L.C. Hartmann, G.L. Keeney, W.L. Lingle, T.J. Christianson, B. Varghese, D. Hillman, A.L. Oberg, P.S. Low, Folate receptor overexpression is associated with poor outcome in breast cancer, *Int. J. Cancer* 121 (5) (2007) 938–942.
- [22] T.A. Halgren, Merck molecular force field .1. Basis, form, scope, parameterization, and performance of MMFF94, *J. Comput. Chem.* 17 (5–6) (1996) 490–519.
- [23] M.J.S. Dewar, E.G. Zoebisch, E.F. Healy, J.J.P. Stewart, The development and use of quantum-mechanical molecular-models .76. Am1 - a new general-purpose quantum-mechanical molecular-model, *J. Am. Chem. Soc.* 107 (13) (1985) 3902–3909.
- [24] R. Fletcher, C.M. Reeves, Function minimization by conjugate gradients, *Comput. J.* 7 (2) (1964) 149–&.
- [25] X. Gao, S.M. Wang, B.L. Wang, S.Y. Deng, X.X. Liu, X.N. Zhang, L.L. Luo, R.R. Fan, M.L. Xiang, C. You, Y.Q. Wei, Z.Y. Qian, G. Guo, Improving the anti-ovarian cancer activity of docetaxel with biodegradable self-assembly micelles through various evaluations, *Biomaterials* 53 (2015) 646–658.
- [26] B.R. Brooks, C.L. Brooks, A.D. Mackerell, L. Nilsson, R.J. Petrella, B. Roux, Y. Won, G. Archontis, C. Bartels, S. Boresch, A. Caffisch, L. Caves, Q. Cui, A.R. Dinner, M. Feig, S. Fischer, J. Gao, M. Hodoscek, W. Im, K. Kuczera, T. Lazaridis, J. Ma, V. Ovchinnikov, E. Paci, R.W. Pastor, C.B. Post, J.Z. Pu, M. Schaefer, B. Tidor, R. M. Venable, H.L. Woodcock, X. Wu, W. Yang, D.M. York, M. Karplus, CHARMM: the biomolecular simulation program, *J. Comput. Chem.* 30 (10) (2009) 1545–1614.
- [27] K. Inaba, M. Inaba, N. Romani, H. Aya, M. Deguchi, S. Ikehara, S. Muramatsu, R. M. Steinman, Generation of large numbers of dendritic cells from mouse bone marrow cultures supplemented with granulocyte/macrophage colony-stimulating factor, *J. Exp. Med.* 176 (6) (1992) 1693–1702.
- [28] J.F. Lim, H. Berger, I.H. Su, Isolation and activation of murine lymphocytes, *JoVE* 116 (2016).
- [29] J.D. Bailey, A. Shaw, E. McNeill, T. Nicol, M. Diotallevi, S. Chuaiphichai, J. Patel, A. Hale, K.M. Channon, M.J. Crabtree, Isolation and culture of murine bone marrow-derived macrophages for nitric oxide and redox biology, *Nitric Oxide* 100–101 (2020) 17–29.
- [30] G.P. Dunn, C.M. Koebel, R.D. Schreiber, Interferons, immunity and cancer immunoeediting, *Nat. Rev. Immunol.* 6 (11) (2006) 836–848.
- [31] F. Balkwill, Tumour necrosis factor and cancer, *Nat. Rev. Canc.* 9 (5) (2009) 361–371.
- [32] J. Matic, J. Deeg, A. Scheffold, I. Goldstein, J.P. Spatz, Fine tuning and efficient T cell activation with stimulatory aCD3 nanoarrays, *Nano Lett.* 13 (11) (2013) 5090–5097.
- [33] D.G. DeNardo, B. Ruffell, Macrophages as regulators of tumour immunity and immunotherapy, *Nat. Rev. Immunol.* 19 (6) (2019) 369–382.
- [34] B. Ruffell, L.M. Coussens, Macrophages and therapeutic resistance in cancer, *Canc. Cell* 27 (4) (2015) 462–472.
- [35] L. Cassetta, J.W. Pollard, Targeting macrophages: therapeutic approaches in cancer, *Nature reviews, Drug discovery* 17 (12) (2018) 887–904.
- [36] A. Sica, A. Mantovani, Macrophage plasticity and polarization: in vivo veritas, *J. Clin. Invest.* 122 (3) (2012) 787–795.
- [37] N. Shimasaki, A. Jain, D. Campana, NK cells for cancer immunotherapy, *Nature reviews, Drug discovery* 19 (3) (2020) 200–218.
- [38] S. Ishigami, S. Natsugoe, K. Tokuda, A. Nakajo, X. Che, H. Iwashige, K. Aridome, S. Hokita, T. Aikou, Prognostic value of intratumoral natural killer cells in gastric carcinoma, *Cancer* 88 (3) (2000) 577–583.
- [39] A.E. Stenzel, S.I. Abrams, K.B. Moysich, A call for epidemiological research on myeloid-derived suppressor cells in ovarian cancer: a review of the existing immunological evidence and suggestions for moving forward, *Front. Immunol.* 10 (2019) 1608.
- [40] A. Toker, L.T. Nguyen, S.C. Stone, S.Y.C. Yang, S.R. Katz, P.A. Shaw, B.A. Clarke, D. Ghazarian, A. Al-Habeeb, A. Easson, W.L. Leong, D.R. McCready, M. Reedijk, C. J. Guidos, T.J. Pugh, M.Q. Bernardini, P.S. Ohashi, Regulatory T cells in ovarian cancer are characterized by a highly activated phenotype distinct from that in melanoma, *Clin. Canc. Res.* 24 (22) (2018) 5685–5696.
- [41] J. Galon, D. Bruni, Tumor immunology and tumor evolution: intertwined histories, *Immunity* 52 (1) (2020) 55–81.
- [42] M.C. Ochoa, J. Fioravanti, I. Rodriguez, S. Hervas-Stubbs, A. Azpilikueta, G. Mazzolini, A. Gurdip, J. Prieto, J. Pardo, P. Berraondo, I. Melero, Antitumor immunotherapeutic and toxic properties of an HDL-conjugated chimeric IL-15 fusion protein, *Canc. Res.* 73 (1) (2013) 139–149.
- [43] T. Kishida, H. Asada, Y. Itokawa, F.D. Cui, M. Shin-Ya, S. Gojo, K. Yasutomi, Y. Ueda, H. Yamagishi, J. Imanishi, O. Mazda, Interleukin (IL)-21 and IL-15 genetic transfer synergistically augments therapeutic antitumor immunity and promotes regression of metastatic lymphoma, *Mol. Ther.* 8 (4) (2003) 552–558.
- [44] K.C. Conlon, M.D. Miljkovic, T.A. Waldmann, Cytokines in the treatment of cancer, *J. Interferon Cytokine Res.* 39 (1) (2019) 6–21.
- [45] J. Shi, P.W. Kantoff, R. Wooster, O.C. Farokhzad, Cancer nanomedicine: progress, challenges and opportunities, *Nat. Rev. Canc.* 17 (1) (2017) 20–37.
- [46] A. Gardner, B. Ruffell, Dendritic cells and cancer immunity, *Trends Immunol.* 37 (12) (2016) 855–865.
- [47] A. Puig-Kroger, E. Sierra-Filardi, A. Dominguez-Soto, R. Samaniego, M.T. Corcuera, F. Gomez-Aguado, M. Ratnam, P. Sanchez-Mateos, A.L. Corbi, Folate receptor beta is expressed by tumor-associated macrophages and constitutes a marker for M2 anti-inflammatory/regulatory macrophages, *Canc. Res.* 69 (24) (2009) 9395–9403.
- [48] S. Chada, R. Ramesh, A.M. Mhashilkar, Cytokine- and chemokine-based gene therapy for cancer, *Curr. Opin. Mol. Therapeut.* 5 (5) (2003) 463–474.
- [49] H. Yin, R.L. Kanasty, A.A. Eltoukhy, A.J. Vegas, J.R. Dorkin, D.G. Anderson, Non-viral vectors for gene-based therapy, *Nat. Rev. Genet.* 15 (8) (2014) 541–555.
- [50] M. Kullberg, R. McCarthy, T.J. Anchordoquy, Systemic tumor-specific gene delivery, *J. Contr. Release : official journal of the Controlled Release Society* 172 (3) (2013) 730–736.
- [51] M.J. Mitchell, M.M. Billingsley, R.M. Haley, M.E. Wechsler, N.A. Peppas, R. Langer, Engineering precision nanoparticles for drug delivery, *Nature reviews, Drug discovery* 20 (2) (2021) 101–124.